Spin stripe dimerization in the $t-J$ model.

O.P. Sushkov
School of Physics, University of New South Wales,
Sydney 2052, Australia

In the present work we demonstrate that the spin columnar dimerized phase (conducting spin stripe liquid) is stable at doping $x_{c1} < x < x_{c2}$. At $x < x_{c1}$ the system undergoes phase transition to the Neel state, and at $x > x_{c2}$ it is Normal Fermi liquid. At $t/J = 3$ the critical concentrations are $x_{c1} \approx 0.09$ and $x_{c2} \sim 0.36$. To prove stability of the stripe phase and to calculate critical concentrations we employ two approaches. The first one is more technically involved, and it gives more accurate value of the critical concentration. The approach is based on the calculation of the magnon Green's function. Imaginary poles in the Green's function indicate transition to the Neel state. The second approach consists in direct comparison of ground state energies of the Neel state and the columnar dimerized state. Both approaches demonstrate stability of the spin stripe phase and give close values of the critical concentrations.

I. INTRODUCTION

It is widely believed that the 2D $t-J$ model is relevant to the low energy physics of high-temperature superconductors. This is why investigation of this model is of great interest both for theory and experiment. In spite of great efforts during more than a decade there is no full understanding of the phase diagram of the $t-J$ model, however some facts are well established. At zero doping the model is equivalent to the Heisenberg model on a square lattice which has long range Neel order[1]. Doping by holes destroys the order. A simplified picture of noninteracting holes leads to the Neel state instability with respect to spirals at arbitrary small but finite doping[2]. However more sophisticated numerical calculations which take into account renormalization of the hole Green's function under the doping indicate that the Neel order is stable below some critical hole concentration x_{c1}[3]. In the Neel phase ($x < x_{c1}$), in all waves except s-wave, there is magnon mediated superconducting pairing between holes.[4]. It is also clear that at very small hopping there is phase separation in the model because separation leads to reduction of the number of destroyed antiferromagnetic links[5]

The purpose of the present work is to elucidate spin structure of the ground state at $x > x_{c1}$. The most important hint comes from experiment: indications of stripes in the high-T_c materials[6]. Another important hint is a remarkable stability of the spin dimerized phase in the frustrated $J_1 - J_2$ model. The idea of such state for this model was first formulated by Read and Sachdev[7], and was then confirmed by further work[8,9]. The stability of such a configuration implies that the lattice symmetry is spontaneously broken and the ground state is four-fold degenerate. Such a route towards quantum disorder is known rigorously to take place in one dimension, where the Lieb-Schultz-Mattis (LSM) theorem guarantees that a gapped phase always breaks the translational symmetry[10]. Some time ago Affleck suggested that the LSM theorem can be extended to higher dimensions, and the gapped states of quantum systems necessarily break the discrete symmetries of the lattice[11]. The example of the $J_1 - J_2$ model provides further support for this idea.

There have been several attempts to consider the spin-dimerized phase in a doped Heisenberg antiferromagnet. For this purpose Affleck and Marston[12] analyzed Hubbard-Heisenberg model in the weak-coupling regime, Grilli, Castellani and G. Kotliar[13] considered $SU(N)$, $N \to \infty$, $t-J$ model, and very recently Vojta and Sachdev[14] considered $Sp(2N)$, $N \to \infty$, $t-J$ model. These works indicated a stability of the spin-dimerized phase in some region of parameters, providing a very important guiding line. However relevance of these results to "physical regime" of the $t-J$ model remained unclear. Stability of the spin-dimer order for the $t-J$ model has been demonstrated in the paper[15]. The only small parameter used in the analysis was hole concentration with respect to the half filling. In the present work we continue studies in the same direction applying various techniques. To be confident in the results we prove stability of the dimer phase by two independent methods: 1) Calculation of the magnon Green's function in the dimerized phase (Green Function Method), 2) Comparison of the ground state energies of the doped Neel state and the dimerized state (Direct Energy Method). The second approach is very simple physically and technically. The first approach is more technically involved, but it allows us to calculate the critical concentration more precisely.

To incorporate some experimental data we consider $t-t'-t''-J$ model defined by the following Hamiltonian

$$H = -t\sum_{\langle ij\rangle\sigma} c^\dagger_{i\sigma}c_{j\sigma} - t'\sum_{\langle ij_1\rangle\sigma} c^\dagger_{i\sigma}c_{j_1\sigma} - t''\sum_{\langle ij_2\rangle\sigma} c^\dagger_{i\sigma}c_{j_2\sigma} + \sum_{\langle ij\rangle\sigma} J_{ij}\left(\mathbf{S}_i\mathbf{S}_j - \frac{1}{4}n_i n_j\right). \quad (1)$$

$c^\dagger_{i\sigma}$ is the creation operator of an electron with spin σ ($\sigma =\uparrow,\downarrow$) at site i of the two-dimensional square lattice. The $\langle ij\rangle$ represents nearest neighbor sites, $\langle ij_1\rangle$ - next nearest neighbor (diagonal), and $\langle ij_2\rangle$ represents next next nearest sites. The spin operator is $\mathbf{S}_i = \frac{1}{2}c^\dagger_{i\alpha}\sigma_{\alpha\beta}c_{i\beta}$ and the number density operator is $n_i = \sum_\sigma c^\dagger_{i\sigma}c_{i\sigma}$. The $c^\dagger_{i\sigma}$ operators act in the Hilbert space with no double electron occupancy. Antiferromagnetic interactions $J_{ij} > 0$ are arranged in a stripe pattern shown in Fig. 1: solid links correspond to $J_{ij} = J_\perp = J(1+\delta)$, and dashed links correspond to $J_{ij} = j = J(1-\delta)$.

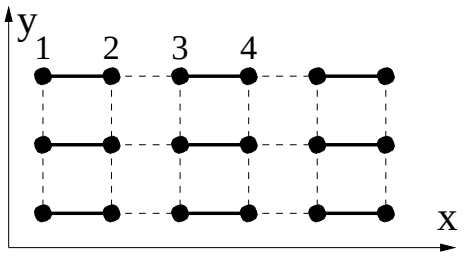

FIG. 1. *Stripe spin dimerization on square lattice. Solid links correspond to $J_\perp = J(1+\delta)$, and dashed links correspond to $j = J(1-\delta)$*

For real cuprates the antiferromagnetic interaction is isotropic, $\delta = 0$. However for theoretical analysis of the magnon Green's function it is convenient to consider nonzero δ and later set $\delta \to 0$. The antiferromagnetic exchange measured in two magnon Raman scattering[16] is $J = 125meV$. Calculation of the hopping matrix elements has been done by Andersen *et al*[17]. They consider a two-plane situation, and the effective matrix elements are slightly different for symmetric and antisymmetric combinations of orbitals between planes. After averaging over these combinations we get: $t = 386meV$, $t' = -105meV$, $t'' = 86meV$. Below we set $J = 1$, in these units

$$t = 3.1, \quad t' = -0.8, \quad t'' = 0.7 \tag{2}$$

These values are confirmed by the analysis[18] of photoemission (PES) data for charge transfer insulator $Sr_2CuO_2Cl_2$. In further numerical estimates we will use the values (2), but we will also consider "pure" $t-J$ model which corresponds to $t' = t'' = 0$.

The rest of the paper is organized as follows. In Sec. II we describe magnon Green's function at zero doping, and remind ideas of the Brueckner technique used in the work. In Sec III the single-hole dispersion and wave function are considered. This section is important for both Green's Function Method and for Direct Energy Method. Sections IV and V contain the main results of the paper: In Sec. IV we demonstrate stabilization of the dimerization by doping using Green's Function Method, and in Sec. V we come to the same conclusion using Direct Energy Method. Sec. VI addresses the quantum phase transition from the dimerized liquid to the Normal Fermi liquid at high doping. In Sec VII we discuss shape of the Fermi surface and distribution of the photoemission intensity. Sec. VIII summarizes the work. Some technical details concerning so called "triple" diagrams are discussed in Appendix.

II. ZERO DOPING

At half filling ($\langle n_i\rangle = 1$) the Hamiltonian (1) is equivalent to a Heisenberg model which has already been studied[8,19]: for $\delta > \delta_c \approx 0.303$ the ground state is a quantum state with gapped spectrum, and for $\delta < \delta_c$ there is spontaneous Neel ordering with gapless spin waves.

In order to study the stability of the dimer phase we first derive an effective Hamiltonian in terms of bosonic operators creating spin-wave triplets (magnons) $t^\dagger_{i\alpha}$, $\alpha = x,y,z$ and fermionic operators creating holes $b^\dagger_\sigma$, $a^\dagger_\sigma$, $\sigma =\uparrow,\downarrow$ from the spin singlets shown in Fig. 1. This Hamiltonian consists of four parts: the spin-wave part H_t, the hole part H_h, the spin-wave-hole interaction H_{th}, and the hole-hole interaction H_{hh}. Let us start from H_t. Similar effective theories have been derived in Refs.[20] and we only present the result:

$$H_t = H_2 + H_3 + H_4 + H_U, \tag{3}$$

$$H_2 = \sum_{\mathbf{k},\alpha}\left\{A_{\mathbf{k}}t^\dagger_{\mathbf{k}\alpha}t_{\mathbf{k}\alpha} + \frac{B_{\mathbf{k}}}{2}\left(t^\dagger_{\mathbf{k}\alpha}t^\dagger_{-\mathbf{k}\alpha} + \text{h.c.}\right)\right\}$$

$$, H_3 = \sum_{1+2=3} \mathrm{R}(\mathbf{k_1},\mathbf{k_2})\epsilon_{\alpha\beta\gamma}t^\dagger_{\mathbf{k_1}\alpha}t^\dagger_{\mathbf{k_2}\beta}t_{\mathbf{k_3}\gamma} + \text{h.c.}$$

$$H_4 = \sum_{1+2=3+4} \mathrm{T}(\mathbf{k_1}-\mathbf{k_3})(\delta_{\alpha\delta}\delta_{\beta\gamma}-\delta_{\alpha\beta}\delta_{\gamma\delta})t^\dagger_{\mathbf{k_1}\alpha}t^\dagger_{\mathbf{k_2}\beta}t_{\mathbf{k_3}\gamma}t_{\mathbf{k_4}\delta}.$$

We also introduce an infinite repulsion on each site, in order to enforce the kinematic constraint $t^\dagger_{i\alpha}t^\dagger_{i\beta}=0$.

$$H_U = U\sum_{i,\alpha\beta} t^\dagger_{i\alpha}t^\dagger_{i\beta}t_{i\beta}t_{i\alpha}, \quad U\to\infty \tag{4}$$

The following definitions are used in (3):

$$\begin{aligned} &A_{\mathbf{k}} = J_\perp + B_{\mathbf{k}}, \\ &B_{\mathbf{k}} = j(\cos k_y - 0.5\cos k_x), \\ &\mathrm{T}(\mathbf{k}) = j(0.25\cos k_x + 0.5\cos k_y), \\ &\mathrm{R}(\mathbf{p},\mathbf{q}) = 0.25j(\sin q_x - \sin p_x). \end{aligned} \tag{5}$$

Throughout the paper we work in the Brillouin zone of the dimerized lattice.

At zero doping ($\langle n_i\rangle = 1$) H_t is an exact mapping of the original Hamiltonian (1). To analyze this case it is enough to apply the Brueckner technique[21,9]. The result for the normal spin-wave Green's function reads:

$$G_N(\mathbf{k},\omega) = \frac{\omega + \tilde{A}_{\mathbf{k}}(-\omega)}{\{\omega+\tilde{A}_{\mathbf{k}}(-\omega)\}\{\omega-\tilde{A}_{\mathbf{k}}(\omega)\}+\tilde{B}^2_{\mathbf{k}}} \tag{6}$$

where

$$\begin{aligned} &\tilde{A}_{\mathbf{k}}(\omega) = A_{\mathbf{k}} + \Sigma^N_4(\mathbf{k}) + \Sigma^{(1)}_{Br}(\mathbf{k},\omega), \\ &\tilde{B}_{\mathbf{k}}(\omega) = B_{\mathbf{k}} + \Sigma^A_4(\mathbf{k}). \end{aligned} \tag{7}$$

Normal Σ^N_4 and anomalous Σ^A_4 self-energies are caused by the quartic interaction H_4 and the most important contribution $\Sigma^{(1)}_{Br}$ comes from the Brueckner diagrams as described in[21]. Strictly speaking there is also some contribution to the self-energy caused by the "triple" interaction H_3. However this contribution is very small (see, e.g. Ref.[9]) and therefore we neglect it.

Expansion of the self-energy in powers of ω near $\omega = 0$ gives quasiparticle residue and spin-wave spectrum

$$\begin{aligned} &Z_{\mathbf{k}} = \left(1 - \frac{\partial\Sigma^{(1)}_{Br}}{\partial\omega}\right)^{-1}, \\ &\omega_{\mathbf{k}} = Z_{\mathbf{k}}\sqrt{[\tilde{A}_{\mathbf{k}}(0)]^2 - \tilde{B_{\mathbf{k}}}^2}. \end{aligned} \tag{8}$$

Expressions for effective Bogoliubov parameters $u_{\mathbf{k}}$ and $v_{\mathbf{k}}$ are given in[21]. The spin-wave gap $\Delta = \omega_{\mathbf{k_0}}$, $\mathbf{k_0} = (0,\pi)$, obtained as a result of a selfconsistent solution of Dyson's equations is plotted in Fig.2 (line at $x = 0$). The critical value of the explicit dimerization (point where the gap vanishes) $\delta_c = 0.298$ is in agreement with results of series expansions[8] and quantum Monte Carlo simulations[19]. The validity of the Brueckner approximation is justified by the smallness of the gas parameter $n_t = \sum_\alpha \langle t^\dagger_{i\alpha}t_{i\alpha}\rangle$. At the critical point $n_t = 0.13$.

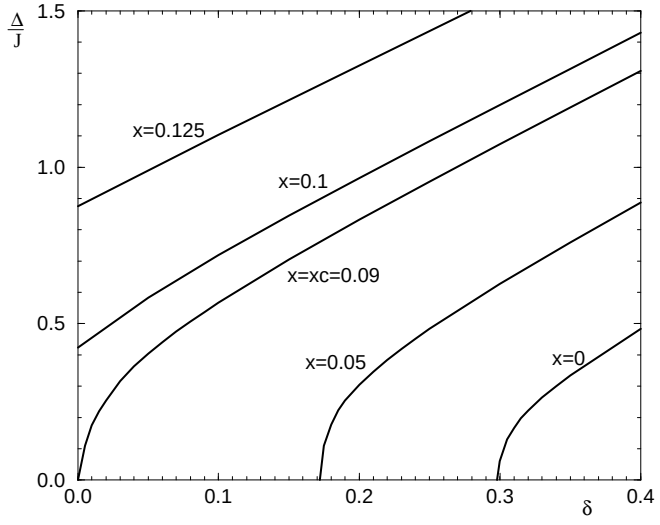

FIG. 2. *The magnon "gap" (centre of gravity of spectral function) as a function of explicit dimerization δ for $t/J = 3$ and different values of hole concentration x, $x = 1 - \langle n_i \rangle$.*

III. SINGLE HOLE DISPERSION

Consider now doping by holes. On the single dimer $|s\rangle$ the hole can exist in symmetric (bonding) and antisymmetric (antibonding) states. Corresponding fermionic operators $b^\dagger_{i\sigma}$, and $a^\dagger_{i\sigma}$ $\sigma =\uparrow,\downarrow$ creating hole from the singlet $|s\rangle_i$ are defined as:

$$b^\dagger_\sigma|s\rangle = \frac{1}{\sqrt{2}}(c^\dagger_{2,\sigma} + c^\dagger_{1,\sigma})|0\rangle, \tag{9}$$
$$a^\dagger_\sigma|s\rangle = \frac{1}{\sqrt{2}}(c^\dagger_{2,\sigma} - c^\dagger_{1,\sigma})|0\rangle,$$

where 1 and 2 numerate the dimer sites.

We will see later that doping suppresses spin quantum fluctuations of the dimerized state so that $n_t = \sum_\alpha \langle t^\dagger_{i\alpha} t_{i\alpha}\rangle$ at $x > x_c$ does not exceed 0.07. This is why we can neglect these fluctuations and consider pure dimerized spin liquid. For comparison we can say that even for spin ladder influence of the quantum fluctuations on the hole dispersion is not strong[22,23] in spite of the fact that in this case $n_t \approx 0.3$.

In leading approximation the wave function of a hole with given quasimomentum is of the form

$$|1\rangle = \frac{1}{\sqrt{N_2}} \sum_n e^{i\mathbf{k}\mathbf{r_n}} b^\dagger_{n\uparrow}|S\rangle, \tag{10}$$

where $|S\rangle$ is the spin dimerized state, index n numerates the dimers and $N_2 = N/2$ is number of sites in the dimerized lattice. We remind that throughout the paper we work in the Brillouin zone of the dimerized lattice. Sometimes the results are transfered to the usual lattice, but then it is specially pointed. The dispersion corresponding to the state (10) can be easily calculated considering all possible hoppings between the dimers. The result is

$$\epsilon_1(\mathbf{k}) = \langle 1|H|1\rangle = -t + (t + t')\cos k_y + (\frac{1}{2}t + t'')\cos k_x + t'\cos k_x \cos k_y + t''\cos 2k_y. \tag{11}$$

There is also an additional t-independent constant in the dispersion

$$e_0 = 1.75J. \tag{12}$$

The constant arises because a hole destroys one spin dimer (this gives $0.75J$) and four links $1/4n_in_j$ (see Hamiltonian (1)). In the present section we ignore e_0 because it gives just a shift of the entire dispersion. However in Section V, calculating total energy of the system we will restore e_0.

The wave function (10) as well as the dispersion (11) are renormalized due to virtual admixture of antibonding states and magnon excitations. Now we calculate this admixture to show that it is small. In this calculation we follow the approach developed earlier for the doped spin ladder[23]. The Hamiltonian (1) admixes following states to the wave function (10)

$$
\begin{aligned}
|2\rangle &= \frac{1}{\sqrt{N_2}}\sum_n e^{i\mathbf{kr_n}} a^\dagger_{n\uparrow}|S\rangle,\\
|3\rangle &= \frac{1}{\sqrt{N_2}}\sum_n e^{i\mathbf{kr_n}} (t^\dagger_n a^\dagger_{n+y})|S\rangle,\\
|4\rangle &= \frac{1}{\sqrt{N_2}}\sum_n e^{i\mathbf{kr_n}} (t^\dagger_n a^\dagger_{n-y})|S\rangle,\\
|5\rangle &= \frac{1}{\sqrt{N_2}}\sum_n e^{i\mathbf{kr_n}} (t^\dagger_n a^\dagger_{n+x})|S\rangle,\\
|6\rangle &= \frac{1}{\sqrt{N_2}}\sum_n e^{i\mathbf{kr_n}} (t^\dagger_n a^\dagger_{n-x})|S\rangle,\\
|7\rangle &= \frac{1}{\sqrt{N_2}}\sum_n e^{i\mathbf{kr_n}} (t^\dagger_n b^\dagger_{n+x})|S\rangle,\\
|8\rangle &= \frac{1}{\sqrt{N_2}}\sum_n e^{i\mathbf{kr_n}} (t^\dagger_n b^\dagger_{n-x})|S\rangle,\\
|9\rangle &= \frac{1}{\sqrt{N_2}}\sum_n e^{i\mathbf{kr_n}} (t^\dagger_n b^\dagger_{n+x+y})|S\rangle,\\
|10\rangle &= \frac{1}{\sqrt{N_2}}\sum_n e^{i\mathbf{kr_n}} (t^\dagger_n b^\dagger_{n+x-y})|S\rangle,\\
|11\rangle &= \frac{1}{\sqrt{N_2}}\sum_n e^{i\mathbf{kr_n}} (t^\dagger_n b^\dagger_{n-x+y})|S\rangle,\\
|12\rangle &= \frac{1}{\sqrt{N_2}}\sum_n e^{i\mathbf{kr_n}} (t^\dagger_n b^\dagger_{n-x-y})|S\rangle,\\
|13\rangle &= \frac{1}{\sqrt{N_2}}\sum_n e^{i\mathbf{kr_n}} (t^\dagger_n a^\dagger_{n+x+y})|S\rangle,\\
|14\rangle &= \frac{1}{\sqrt{N_2}}\sum_n e^{i\mathbf{kr_n}} (t^\dagger_n a^\dagger_{n+x-y})|S\rangle,\\
|15\rangle &= \frac{1}{\sqrt{N_2}}\sum_n e^{i\mathbf{kr_n}} (t^\dagger_n a^\dagger_{n-x+y})|S\rangle,\\
|16\rangle &= \frac{1}{\sqrt{N_2}}\sum_n e^{i\mathbf{kr_n}} (t^\dagger_n a^\dagger_{n-x-y})|S\rangle,\\
|17\rangle &= \frac{1}{\sqrt{N_2}}\sum_n e^{i\mathbf{kr_n}} (t^\dagger_n b^\dagger_{n+y})|S\rangle,\\
|18\rangle &= \frac{1}{\sqrt{N_2}}\sum_n e^{i\mathbf{kr_n}} (t^\dagger_n b^\dagger_{n-y})|S\rangle.
\end{aligned}
\tag{13}
$$

The state $|2\rangle$ is similar to $|1\rangle$ with replacement of bonding orbital to the antibonding one. The states $|3\rangle - |18\rangle$ describe excited triplet (magnon) on the dimer n and a hole on the one of the closest dimers, for example $n+x$ denotes the dimer on the right, $n+x+y$ denotes the up-right dimer, etc. The brackets $(t^\dagger a^\dagger)$ denote that spins of the magnon and the hole are combined to the total spin 1/2 and z-projection 1/2: $|1/2, 1/2\rangle$. Calculation of matrix elements of the Hamiltonian is straightforward. The diagonal matrix elements are

$$
\begin{aligned}
\langle 2|H|2\rangle &= t + (t-t')\cos k_y - (\frac{1}{2}t - t'')\cos k_x - t'\cos k_x \cos k_y + t''\cos 2k_y,\\
\langle 3|H|3\rangle &= \langle 4|H|4\rangle = t + J_\perp - j/2,\\
\langle 5|H|5\rangle &= \langle 6|H|6\rangle = t + J_\perp - j/4,\\
\langle 7|H|7\rangle &= \langle 8|H|8\rangle = -t + J_\perp - j/4,\\
\langle 9|H|9\rangle &= \langle 10|H|10\rangle = \langle 11|H|11\rangle = \langle 12|H|12\rangle = -t + J_\perp,\\
\langle 13|H|13\rangle &= \langle 14|H|14\rangle = \langle 15|H|15\rangle = \langle 16|H|16\rangle = t + J_\perp,\\
\langle 17|H|17\rangle &= \langle 18|H|18\rangle = -t + J_\perp - j/2.
\end{aligned}
\tag{14}
$$

The nonzero nondiagonal matrix elements are

$$
\begin{aligned}
\langle 2|H|1\rangle &= -i\frac{t}{2}\sin k_x,\\
\langle 3|H|1\rangle &= \langle 4|H|1\rangle^* = \frac{\sqrt{3}}{2}(t-t') + \frac{\sqrt{3}}{4}je^{ik_y},\\
\langle 5|H|1\rangle &= \langle 6|H|1\rangle^* = -\frac{\sqrt{3}}{4}(t-2t'') - \frac{\sqrt{3}}{8}je^{ik_x},\\
\langle 7|H|1\rangle &= -\langle 8|H|1\rangle^* = -\frac{\sqrt{3}}{4}t + \frac{\sqrt{3}}{8}je^{ik_x},\\
\langle 9|H|1\rangle &= \langle 10|H|1\rangle = -\langle 11|H|1\rangle = -\langle 12|H|1\rangle = -\frac{\sqrt{3}}{4}t',\\
\langle 13|H|1\rangle &= \langle 14|H|1\rangle = \langle 15|H|1\rangle = \langle 16|H|1\rangle = -\frac{\sqrt{3}}{4}t',\\
\langle 5|H|2\rangle &= -\langle 6|H|2\rangle^* = \frac{\sqrt{3}}{4}t + \frac{\sqrt{3}}{8}je^{ik_x},\\
\langle 7|H|2\rangle &= \langle 8|H|2\rangle^* = \frac{\sqrt{3}}{4}(t+t'') - \frac{\sqrt{3}}{8}je^{ik_x},\\
\langle 9|H|2\rangle &= \langle 10|H|2\rangle = \langle 11|H|2\rangle = \langle 12|H|2\rangle = \frac{\sqrt{3}}{4}t',\\
\langle 13|H|2\rangle &= \langle 14|H|2\rangle = -\langle 15|H|2\rangle = -\langle 16|H|2\rangle = \frac{\sqrt{3}}{4}t',\\
\langle 17|H|2\rangle &= \langle 18|H|2\rangle^* = \frac{\sqrt{3}}{2}(t+t') + \frac{\sqrt{3}}{4}je^{ik_y},\\
\langle 4|H|3\rangle &= -\frac{(t-t')}{2}e^{-ik_y},\\
\langle 18|H|17\rangle &= -\frac{(t+t')}{2}e^{-ik_y}.
\end{aligned}
\tag{15}
$$

Diagonalization of the Hamiltonian matrix can be performed numerically. This gives the quasiparticle dispersion $\epsilon_{\mathbf{k}}$ and the quasiparticle residue $Z_{\mathbf{k}}^{(h)}$ which by definition is equal to the weight of the state $|1\rangle$ (see eq. (10) in the exact wave function[24]. The minimum energy for different sets of parameters is shown in the fifth column of the Table I. We remind that we use units $J = 1$. In the last column we show position of the minimum. For comparison we also display the minimum value of ϵ_1 (see eq. (11)), which always is at $\mathbf{p}_0 = (\pi, \pi)$.

Table I.

t	t'	t''	$\epsilon_{1,min}$	ϵ_{min}	$\mathbf{p}_0$
3.1	-0.8	0.7	-7.75	-9.70	$(\pi, 0.82\pi)$
3.	0.	0.	-7.50	-9.03	(π, π)
2.	0.	0.	-5.0	-5.95	(π, π)
1.	0.	0.	-2.5	-2.91	(π, π)

Let us denote the hole concentration by $x = n/N$, where n is number of holes, and N is number of sites. Hence on-site electron occupation number is $\langle n_i\rangle = 1 - x$. Concentration of holes in terms of the dimerized lattice is two times

larger $n/(0.5N) = 2x$. At this stage we neglect interaction of holes between themselves, hence we consider them as an ideal Fermi gas, and the Fermi surface can be easily found from the condition

$$2\int \frac{dk_x dk_y}{(2\pi)^2} = 2x, \tag{16}$$

where integration is performed inside the Brillouin zone of the dimerized lattice. The Fermi surface at $x = 0.1$ and hopping parameters given in (2) is shown in Fig. 3 by solid line.

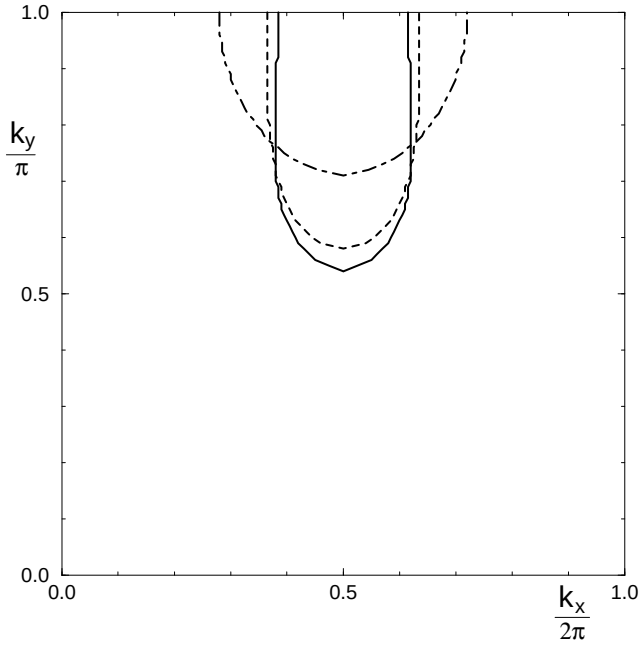

FIG. 3. *Fermi surface of the dimerized spin liquid at doping $x = 0.1$. Dot-dashed line corresponds to $t/J = 3$, $t', t'' = 0$, solid and dashed lines correspond to the set of parameters from (2). Solid line gives Fermi surface found with "exact" dispersion as it is described in Section III. Dashed line corresponds to the bare dispersion (11). We put $k_x/2\pi$ along the horizontal axis and k_y/π along the vertical axis, so the picture corresponds to a quadrant of the Brillouin zone of the original lattice.*

We stress that in this figure we put $k_x/2\pi$ along the horizontal axis and k_y/π along the vertical axis. It means that the picture corresponds to a quadrant of the Brillouin zone of the original lattice. The Fermi surface corresponding to the bare dispersion (11) is shown by the dashed line. The two curves are very close and this proves that the dispersion renormalization is small. The wave function renormalization is also not large and the quasiparticle residue is close to unity: it is $Z^{(h)} = 0.83$ at the bottom of the band, and at the Fermi surface $Z^{(h)} = 0.80$. So admixture of the states (13) to the bare state $|1\rangle$ is relatively small. In this admixture the states $|3\rangle$, $|4\rangle$, $|7\rangle$, and $|8\rangle$ clearly dominate. In a reasonable approximation the wave function can be written as

$$\psi \approx 0.9|1\rangle - 0.22(|3\rangle + |4\rangle - |7\rangle + |8\rangle). \tag{17}$$

Admixture of other components is even smaller. For comparison in Fig. 3 we show also by dot-dashed line the Fermi surface for "pure" $t - J$ model ($t/J = 3$, $t' = t'' = 0$, doping is the same, $x = 0.1$). We see that the additional hoppings influence substantially shape of the Fermi surface.

IV. THE SPIN-WAVE-HOLE INTERACTION. STABILIZATION OF THE DIMER ORDER

The magnon-hole interaction H_{th} can be easily calculated in the way similar to that for doped spin-ladder[22,23]. This interaction consists of two parts. The first one is interaction of a hole and a magnon positioned at different dimers. This is a relatively weak interaction which can be neglected[22,23]. The second part, which gives the main effect, comes from the constraint that a hole and a magnon can not coexist at the same dimer: $t^\dagger_{i\alpha} b^\dagger_{i\sigma} = t^\dagger_{i\alpha} a^\dagger_{i\sigma} = 0$. To deal with this constraint we introduce, similarly to (4), an infinite repulsion

$$H_{U1} = U \sum_{i,\alpha\sigma} t^\dagger_{i\alpha} t_{i\alpha} (b^\dagger_{i\sigma} b_{i\sigma} + a^\dagger_{i\sigma} a_{i\sigma}), \quad U \to \infty. \tag{18}$$

The exact hole-magnon scattering amplitude caused by this interaction can be found via Bethe-Salpeter equation shown in Fig.4a.

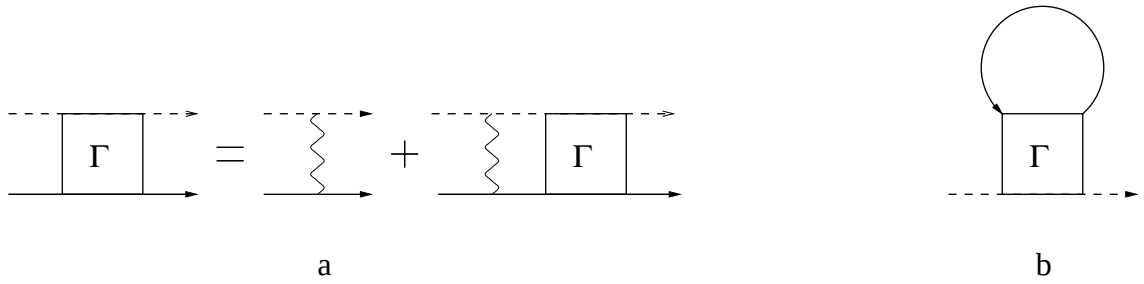

FIG. 4. *(a) Bethe-Salpeter equation for hole-magnon scattering vertex* Γ*. Solid line corresponds to the hole and dashed line to the magnon. (b) Brueckner contribution to the magnon self energy.*

This scattering amplitude is similar to that for magnon-magnon scattering[21]. Solution of the Bethe-Salpeter equation gives

$$\Gamma(E, \mathbf{k}) = -\left(\sum_{\mathbf{q}} \frac{Z_{\mathbf{q}} u^2_{\mathbf{q}}}{E - \omega_{\mathbf{q}} - \epsilon_1(\mathbf{k} - \mathbf{q})} \right)^{-1}, \tag{19}$$

where E and $\mathbf{k}$ is total energy and total momentum of the incoming particles. It has been demonstrated in the previous section that the renormalized hole dispersion $\epsilon_{\mathbf{k}}$ is close to the bare one $\epsilon_1(\mathbf{k})$. This is why we use in eq. (19) the bare dispersion (11).

We remind that concentration of holes in terms of the dimerized lattice is $2x \ll 1$, and this is the gas parameter of the magnon-hole Brueckner approximation. In the previous section we have shown that the holes are concentrated in the pocket in the vicinity of $\mathbf{p_0} = (\pi, \pi)$. Therefore the magnon normal self-energy described by the diagram Fig. 4b is

$$\Sigma^{(2)}_{Br}(\mathbf{k}, \omega) = 2x\Gamma[\omega + \epsilon_1(\mathbf{p_0}), \mathbf{k} + \mathbf{p_0}] \tag{20}$$

It is instructive to consider first the limit which allows an analytical solution: $j \ll J_\perp$, $\sqrt{2}\pi x \ll 1$. Bare magnon dispersion in this case is $\omega_{\mathbf{k}} \approx J_\perp + j(\cos k_y - 0.5 \cos k_x)$ and hence the integrals in (19,20) can be calculated analytically with logarithmic accuracy. This gives

$$\Sigma^{(2)}_{Br}(\mathbf{k}, \omega) \approx \frac{2\sqrt{2}\pi x(t + j)}{\ln(12.5/\mu) + i\pi\theta(\delta\omega)}, \tag{21}$$

where

$$\delta\omega = \frac{1}{t + j} \left[\omega - \omega_{\mathbf{k}} + \frac{j}{t + j} (\omega_{\mathbf{k}} - \omega_{\mathbf{k_0}}) \right], \tag{22}$$
$$\mu = \max(|\delta\omega|, \sqrt{2}\pi x),$$

and $\theta(\delta\omega)$ is a step function. The magnon Green's function is

$$G(\mathbf{k}, \omega) = \frac{1}{\omega - \omega_{\mathbf{k}} - \Sigma^{(2)}_{Br}(\mathbf{k}, \omega)}. \tag{23}$$

For illustration the spectral function $ImG(\omega)$ at $\mathbf{k} = \mathbf{k_0} = (0, \pi)$, $t/j = 3$ and different x is plotted in Fig.5.

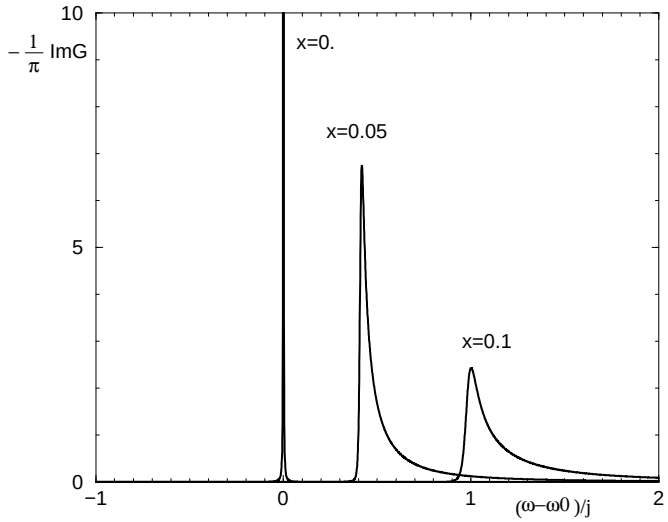

FIG. 5. *Magnon spectral density at* $\mathbf{k} = \mathbf{k_0} = (0, \pi)$ *in the limit* $J_\perp \gg j$, $t/j = 3$, *and different hole concentrations.*

There are several conclusions from formula (21) and Fig. 5: 1) doping pushes the spin-wave spectrum up, 2) the effect is increasing with hopping t, 3) finite width appears, 4) there is only a logarithmic dependence on the infrared cutoff. Let us stress the importance of the point (4). It means that the effect is practically independent of the long-range dynamics. Moreover, near the critical point ($\Delta = 0$) the situation is even better: the spin-wave spectrum is linear and even the logarithmic divergence disappears. Thus in the 2D case there is separation of scales which justifies Brueckner approximation. If we tried to apply the described approach to the 1D case (say a doped spin ladder) we would get into trouble: power infrared divergence appears in Brueckner diagram and hence there is no justification for gas approximation. Let us also comment on the point (3) (width). There is also a "triple" contribution to the magnon self-energy shown in Fig. 6a,b.

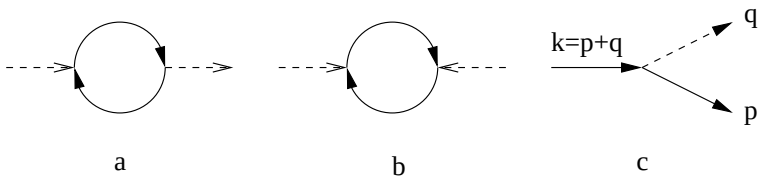

FIG. 6. *(a) Normal "triple" contribution to the magnon self energy. (b) Anomalous "triple" contribution to the magnon self energy. (c) hole-magnon "triple" vertex.*

This is a long-range contribution, and it can be shown that it does not influence position of the critical point ($\Delta = 0$) in linear in x approximation. This fact will be proved in Appendix and this is why here we neglect the "triple" diagrams. However note that these diagrams influence the width of the magnon spectral function.

In the general case there are two contributions to the Brueckner self-energy: $\Sigma^{(1)}_{Br}$, which is due to the magnon-magnon constraint, and $\Sigma^{(2)}_{Br}$ which is due to the magnon-hole constraint. To find the spin wave spectrum one has to solve selfconsistently Dyson's equation for Green's function (6), as it is described in Ref.[21]. Results for the spin-wave "gap" Δ as a function of explicit dimerization δ for different hole concentrations x and $t/J = 3$ are plotted in Fig. 2. These curves are practically independent of the longer range hoppings t' and t''. Strictly speaking at $x \neq 0$ the Δ is not a gap because of the large decay width. What we plot is the position of the center of gravity of the magnon spectral function. However at $\Delta \to 0$ the width vanishes, and therefore the critical regime is uniquely defined.

It is clear from Fig.2 that at $t/J = 3$ and $x > x_{c1} \approx 0.090$ the "gap" remains finite even at $\delta = 0$. This is regime of spontaneous dimerization. Critical concentrations for other values of t/J are presented in Table II.

Table II.

t/J	1	2	3
x_{c1}	0.132	0.106	0.090

Thus the doping stabilizes the dimerized phase. The larger the hopping t, the stronger the effect of stabilization. (The same follows from eq. (21).) This statement is true only if $t/J \lesssim 10$. At $t/J \sim 10$ there is a crossover to quasiparticles with higher spin (hole-magnon bound states)[23] which indicates transition to the Nagaoka regime. The small parameter of the Brueckner approximation is concentration of holes in the dimerized lattice: $2x$. Therefore at $t/J = 3$ one should expect $\sim 20\%$ accuracy in calculation of x_{c1}. Note that the value of x_{c1} is close to that found in[3] from the Neel state.

Another important gas parameter is density of spin fluctuations n_t. It also proved to be small: At the critical point, $\delta = 0$, $x = x_c = 0.09$, the density is $n_t \approx 0.07$.

V. DIRECT COMPARISON OF GROUND STATE ENERGIES OF THE NEEL STATE AND THE SPIN DIMERIZED STATE

In the previous section we have demonstrated quantum phase transition from the Neel state to the spin dimerized state at some critical hole concentration x_{c1}. We calculated the magnon Green's function in the dimerized phase, and the transition point was identified as the point where the magnon gap vanishes. This is a rigorous approach which allows to determine x_{c1} with relatively high precision ($\sim 20\%$), however it is rather involved technically. An alternative method is direct comparison of the ground state energies of these two states. This is a very simple method which does not require introduction of the explicit dimerization. So throughout this section $\delta = 0$.

The energy per site for the undoped Neel state is $-1.17 = -0.67 - 0.5$, where the first term is Heisenberg energy (see e. g. Ref.[25]), and the second contribution comes from the $-1/4 n_i n_j$ term in the Hamiltonian (1). We remind that in our units J=1. In this section we consider only "pure" $t - J$ model, i. e. $t' = t'' = 0$. Energy of a single hole injected into the Neel background is $-3.17t + 2.83t^{0.27} + 1$, see e. g. Ref.[26], where the last term comes from the $-1/4 n_i n_j$ term in the Hamiltonian (1). Therefore in linear in x approximation energy of the doped Neel state is

$$E_{Neel}/N = -1.17 + (-3.17t + 2.83t^{0.27} + 1)x. \tag{24}$$

Energy of the undoped columnar dimerized state without account of quantum fluctuations is $(-0.375 - 0.5)N$, where -0.375 is Heisenberg energy and -0.5 comes from the $-1/4 n_i n_j$ term in the Hamiltonian (1). Quantum fluctuations push this energy down. Using perturbation theory one can find that in linear in n_t (triplet density) approximation this shift is $\sim -0.5 n_t N$. According to previous section at the critical point $n_t \approx 0.07$ and therefore the shift is tiny. Energy of a single hole injected into the spin dimerized background has been found in section III, $\epsilon = e_0 + \epsilon_{min}$, where e_0 is given by eq. (12) and the values of ϵ_{min} are presented in Table I. For $1 \le t \le 4$ one can fit ϵ_{min} as $\epsilon_{min} \approx -3.0t$. Altogether this gives following energy of the doped dimerized state (linear in x approximation)

$$E_{Dimer}/N = -0.91 + (-3t + 1.75)x. \tag{25}$$

At $x = 0$ the Neel state energy (24) is lower than that of the dimerized state (25). The critical concentration (the transition point to the dimerized state) is defined by the condition $E_{Neel} = E_{Dimer}$. This gives following values of the critical concentration:

Table III.

t/J	1	2	3
x_{c1}	0.14	0.11	0.10

The values of x_{c1} in Table III are somewhat overestimated. The matter is that the single hole energy for the Neel state is known with high precision, at the same time similar energy for the dimerized state has been found in Section III with trial wave function which contains only 18 components. The true energy is lower than the variational one. To estimate this uncertainty we refer to the doped spin ladder. There is a variational calculation[23] for this system which is similar to to the calculation in Sec. III, and there are also exact numerical simulations[27]. Comparison shows that the variational method underestimate ϵ_{min} (see Table I) by 10-15%. Taking this as an estimate we should replace the term $-3t$ in eq. (25) by $-3.3t$. Then we come to following values of the critical concentration

Table IV.

t/J	1	2	3
x_{c1}	0.12	0.09	0.08

Altogether results for x_{c1} presented in Tables II, and III, IV and derived by absolutely different methods are in remarkable agreement. This gives a very strong confirmation of the phase transition to the columnar spin dimerized state. Physical reason for stability of the spin dimerized state is especially evident after the energy considerations: this is the gain in the hole kinetic energy, it is "easier" to propagate in the dimerized background.

VI. SPIN-DIMER ORDER PARAMETER AND TRANSITION TO THE NORMAL FERMI LIQUID AT HIGH DOPING.

We have discussed the transition to the Neel state at hole concentration $x < x_{c1}$. It is clear that at large x ($x > x_{c2}$) there is a 2nd order phase transition to the normal Fermi liquid. Let us define the spin-dimer order parameter as

$$\rho = \langle \mathbf{S}_2 \mathbf{S}_3 \rangle - \langle \mathbf{S}_1 \mathbf{S}_2 \rangle, \tag{26}$$

where sites 1, 2, and 3 are shown in Fig. 1. For perfect dimerized state $\rho = 3/4$. There are two mechanisms for reduction of the order parameter. The first one is due to spin quantum fluctuations which approximately give $\rho \to 3/4 - n_t$. The second mechanism is direct effect of doping. Naive estimate is $\rho \to 3/4(1-2x)$, however the hole wave function (17) is slightly different from the bare one and because of this the coefficient in the naive formula is slightly renormalized. All together this gives

$$\rho = \frac{3}{4}[1 - 2x(1 + 6\alpha^2)] - n_t, \tag{27}$$

where $\alpha = 0.22$ is the admixture coefficient in eq. (17). This formula is derived in dilute gas approximation, i.e at $2x, n_t \ll 1$, however for an estimate we can extend it to large x. Setting $n_t \sim 0.05$ we find from (27) that ρ vanishes at $x_{c2} \approx 0.36$. We repeat that this is only an estimate because the approach assumes that $2x \ll 1$.

The phase diagram of the $t - J - \delta$ model at zero temperature is presented in Fig. 7

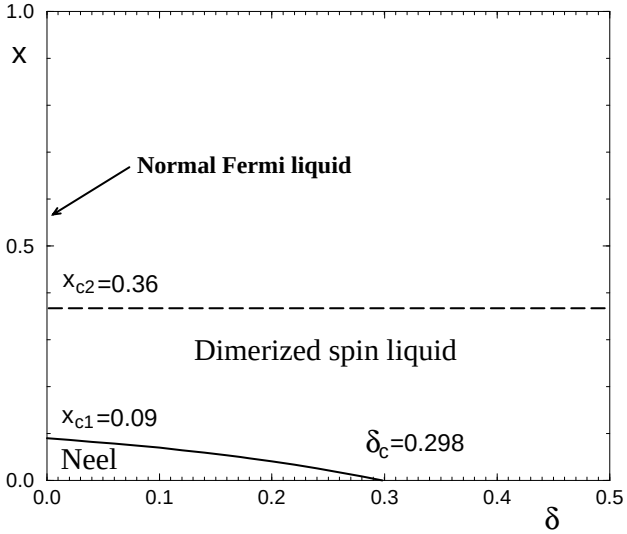

FIG. 7. *Phase diagram of the $t - J - \delta$ model ($t/J = 3$) in the plane doping (x) - explicit dimerization (δ).*

Because of the mobile holes the dimerized spin liquid at $x_{c1} < x < x_{c2}$ is a conducting state. Stability of this state is a very robust effect because it is due to the high energy correlations (typical energy scale $\sim 2t$). There are also low energy effects with typical energy scale $\sim 2tx$ which can lead to hole-hole pairing, charge stripes, etc. We do not consider these effects in the present work because they are secondary with respect to the main one: spin dimerization. However we would like to note that there is a simple mechanism for charge stripes induced by the spin dimers: Because of the anisotropic dispersion, see Fig. 3, the charge response is enhanced at some momentum $\mathbf{p} = (p_x, 0)$. The effect is very sensitive to additional hopping parameters t' and t'', they can further enhance or suppress the response.

VII. SHAPE OF THE FERMI SURFACE AND PES INTENSITY

Shape of the Fermi surface for the dimerized state at the doping $x = 0.1$ and hopping matrix elements from (2) is shown in Fig.3 by the solid line. In this figure we put $k_x/2\pi$ along the horizontal axis and k_y/π along the vertical axis, where $\mathbf{k}$ is defined on the dimerized lattice. In terms of the Brillouin zone of the original lattice this is usual quadrant: $0 \le P_x \le \pi$, $0 \le P_y \le \pi$. To distinguish between the dimerized lattice and the original one we denote by capital letters momenta corresponding to the original lattice: $P_x = k_x/2$, $P_y = k_y$.

In a real sample there are domains with one stripe dimerization and there are domains with stripes rotated by 90^o. Therefore in an experiment one should see two superimposed Fermi surfaces. Corresponding picture for $x = 0.15$ is shown in Fig. 8.

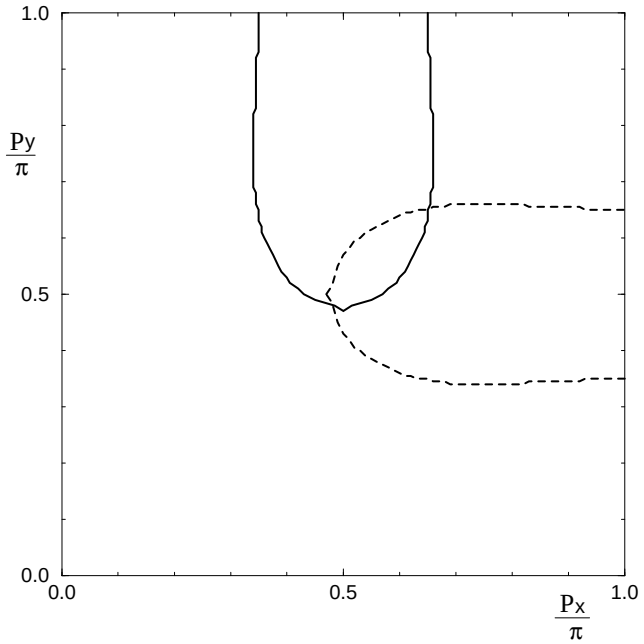

FIG. 8. *Two superimposed Fermi surfaces of the dimerized spin liquid corresponding to different orientations of the stripes. The hole concentration is* $x = 0.15$. *The picture corresponds to a quadrant of the Brillouin zone of the original lattice* $0 \le P_x \le \pi$, $0 \le P_y \le \pi$.

The first impression is that it is very much different from what is usually observed in angular resolved photoemission (PES) experiments, see e. g. Ref.[28] However let us calculate intensity of the photoemission.

The photoeffect operator is of the form

$$\hat{A} = \sum_n c_{i\downarrow} e^{i\mathbf{P}\mathbf{r_n}}, \tag{28}$$

where summation is performed over sites of the square lattice. Amplitude of the hole creation from the dimerized background (oriented as it is shown in Fig. 1) is equal to

$$A = \langle s|b_\uparrow \hat{A}|s\rangle = \cos(P_x/2). \tag{29}$$

Here we have taken into account that according to considerations in Section III wave function of the hole in bonding state is practically unrenormalized. We stress once more that $\mathbf{P}$ is a quasimomentum corresponding to the original lattice. According to (29) intensity of PES spectra ($I \propto A^2$) is dropping quickly as P_x is increasing. If one assumes that the $t - J$ model originates from the single band Hubbard model, then the corrections of the order of t/U to the PES intensity can be calculated in a way suggested in Ref.[18]. This gives

$$I_{\mathbf{P}} \propto \left(\cos\frac{P_x}{2} + \frac{J}{8t}\cos\frac{3P_x}{2} + \frac{J}{4t}\cos\frac{P_x}{2}\cos P_y\right)^2. \tag{30}$$

The Hubbard repulsion U is excluded from this formula using relation $J = 4t^2/U$. According to (30) the PES intensity is strongly asymmetric at the Fermi surface. For example at $x = 0.15$ the intensity at the right top corner of the Fermi

surface, $P_x = 0.66\pi$, $P_y = \pi$ (see Fig. 8) is 3.5 times smaller than that at the left top corner of the Fermi surface, $P_x = 0.34\pi$, $P_y = \pi$. In real cuprate the asymmetry must be even stronger. The reason for further enhancement of the asymmetry is structure factor of the Zhang-Rice singlet. This is quite similar to the well understood situation in the charge transfer insulator $Sr_2CuO_2Cl_2$, see Ref.[18].

Thus the angle resolved photoemission measurements are sensitive only to the "inner" parts (the parts closest to the Γ point: $\mathbf{P} = (0,0)$) of the Fermi surfaces shown in Fig. 8. Shape of this effective "Fermi surface" is very close to what is observed in numerous PES experiments. Another feature which agrees with experiment is width of the "quasiparticle" peak along (1,1) direction: it is always rather big because the peak arises as a superposition of two different peaks corresponding to two different Fermi surfaces.

VIII. CONCLUSIONS

In conclusion, using the dilute gas approximation we have analyzed the phase diagram of the $t-J$ model and the stability of spin-dimerized phase. The main result of the work is phase diagram shown in Fig. 7. Without any explicit dimerization ($\delta = 0$) the spin dimerized phase is stable at hole concentration $x_{c1} < x < x_{c2}$. At $t/J = 3$ the critical concentrations are $x_{c1} \approx 0.09$, $x_{c2} \sim 0.36$. At $x < x_{c1}$ the system undergoes transition to the Neel state, and at $x > x_{c2}$ to the Normal Fermi liquid.

To prove stability of the spin dimerized phase and to calculate critical concentrations we have used two independent approaches. The first one is based on the calculation of the magnon Green's function. The second approach consists in direct comparison of ground state energies of the Neel state and the dimerized state. Both approaches demonstrate stability of the spin dimerized phase and give very close values of the critical concentrations.

ACKNOWLEDGMENTS

I thank V. N. Kotov and M. Yu. Kuchiev for stimulating discussions. I am especially grateful to T. M. Rice who attracted my attention to the direct comparison of the ground state energies.

---

[1] J. Oitmaa and D. D. Betts, Can. J. Phys. **56**, 897 (1971).
[2] B. I. Shraiman and E. D. Siggia, Phys. Rev. Lett., **62**, 1564 (1989).
[3] J. Igarashi and P. Fulde, Phys. Rev. B **45**, 12357 (1992); G. Khaliullin and P. Horsch, Phys. Rev. B **47**, 463 (1993).
[4] V. V. Flambaum, M. Yu. Kuchiev, and O. P. Sushkov, Physica C **227**, 267 (1994); V. I. Belinicher, A. L. Chernyshev, A. V. Dotsenko, and O. P. Sushkov, Phys. Rev. B **51**, 6076 (1995).
[5] V. J. Emery, S. A. Kivelson, and H. Q. Lin, Phys. Rev. Lett., **64**, 475 (1990).
[6] J.M. Tranquada *et al.*, Nature **375**, 561 (1995); S. Wakimoto *et al*, cond-mat/9902201, cond-mat/9902319.
[7] N. Read and S. Sachdev, Phys. Rev. Lett. **62**, 1697 (1989).
[8] M.P. Gelfand, R.R.P. Singh, and D.A. Huse, Phys. Rev. B **40**, 10801 (1989).
[9] V.N. Kotov, J. Oitmaa, O. P. Sushkov, and Zheng Weihong, Phys. Rev. B **60**, 14613 (1999); R. R. P. Singh, Zheng Weihong, C. J. Hamer, and J. Oitmaa, Phys. Rev. B **60**, 7278 (1999).
[10] E. Lieb, T. Schultz, and D. Mattis, Ann. Phys. (N.Y.) **16**, 407 (1961).
[11] I. A. Affleck, Phys. Rev. B **37**, 5186 (1988).
[12] I. Affleck and J. B. Marston, Phys. Rev. B **37**, 3774 (1988).
[13] M. Grilli, C. Castellani, and G. Kotliar, Phys. Rev. B **45**, 10805 (1992).
[14] M. Vojta and S. Sachdev, Phys. Rev. Lett. **83**, 3916 (1999).
[15] O. P. Sushkov, cond-mat/9907400.
[16] Y. Tokura *et al*, Phys. Rev. B **41**, 11657 (1990); M. Greven *et al*, Phys. Rev. Lett. **72** 1096 (1994).
[17] O. K. Andersen *et al*, J. Phys. Chem. Solids **56** 1573 (1995).
[18] O. P. Sushkov, G. Sawatzky, R. Eder, and H. Eskes, Phys. Rev B **56**, 11769 (1997).
[19] N. Katoh and M. Imada, J. Phys. Soc. Jpn. **62**, 3728 (1993); A. W. Sandvik and M. Vekic, J. Low Temp. Phys. **99**, 367 (1995).
[20] S. Sachdev and R.N. Bhatt, Phys. Rev. B **41** 9323 (1990); A.V. Chubukov and T. Jolicoeur, Phys. Rev. B **44**, 12050 (1991).
[21] V.N. Kotov, O.P. Sushkov, W.H. Zheng, and J. Oitmaa, Phys. Rev. Lett. **80**, 5790 (1998); O.P. Sushkov and V.N. Kotov, Phys. Rev. Lett. **81**, 1941 (1998).

[22] R. Eder, Phys. Rev. B **57**, 12823 (1997).
[23] O. P. Sushkov, Phys. Rev. B **60**, 3289 (1999).
[24] Do not mix magnon quasiparticle residue $Z_{\mathbf{k}}$, see (8), and hole quasiparticle residue $Z_{\mathbf{k}}^{(h)}$.
[25] E. Manousakis, Rev. Mod. Phys. **63**, 1 (1991).
[26] E. Dagotto, Rev. Mod. Phys. **66**, 763 (1994); G. Martinez and P. Horsch, Phys. Rev. B **44**, 317 (1991).
[27] M. Troyer, H. Tsunetsugu, and T. M. Rice, Phys. Rev. B **53**, 251 (1996); J. Oitmaa, C. J. Hamer, and Zheng Weihong, Phys. Rev. B **60**, 16364 (1999).
[28] D. S. Marshall *et al.*, Phys. Rev. Lett. **76**, 4841 (1996).

IX. APPENDIX: "TRIPLE" DIAGRAMS

Purpose of the present section is to demonstrate that the "triple" diagrams shown in Fig. 6a,b do not influence position of the critical point x_{c1} found in Section IV. The "triple" vertex is shown in Fig. 6c. In the present section we completely neglect small renormalization of the hole wave function considered in Section III. Therefore, the initial state in Fig. 6c is given by (10) and the final state is

$$|f\rangle = b^\dagger_{p\sigma} t^\dagger_{q\alpha} |S\rangle = \frac{1}{N_2} \sum_n e^{i\mathbf{p}\mathbf{r_n}} b^\dagger_{n\sigma} \sum_m e^{i\mathbf{q}\mathbf{r_m}} t^\dagger_{m\alpha} |S\rangle. \tag{31}$$

Kinematic structure of the vertex is obvious

$$\Gamma_{\mathbf{p},\mathbf{q}} = -iA t^\dagger_{\mathbf{q}\alpha} [b^\dagger_{\mathbf{p}} \sigma_\alpha b_{\mathbf{p}+\mathbf{q}}], \tag{32}$$

where σ_α, $\alpha = 1,2,3$ is vector of Pauli matrices, and $b^\dagger_{\mathbf{p}}$ is the hole wave function in spinor representation. Direct calculation of the matrix element $\langle f|H|1\rangle$ and comparison with (32) gives following value of the coupling constant

$$A = \frac{1}{2}\left[(t + 2t'\cos p_y)\sin p_x + \frac{j}{2}\sin q_x\right]. \tag{33}$$

The normal "triple" magnon self-energy $\Sigma_{3n}(\mathbf{q},\omega)$ is shown in Fig. 6a. Since we are interested in the critical point x_{c1} it is enough to calculate the self energy at zero frequency and at the momentum where the spin-wave gap vanishes: $\mathbf{q} = \mathbf{q}_0 = (0,\pi)$. Straightforward calculation of the loop at $t' = t'' = 0$ gives

$$\Sigma_{3n}(\mathbf{q}_0, 0) = -tx. \tag{34}$$

Unfortunately analytical calculation at the values of t' and t'' from (2) is impossible because at these values the curvature of the hole dispersion along y-direction vanishes. However numerical calculation shows that at $x = 0.1-0.15$ and t', t'' from (2) the "triple" self-energy is by a factor 1.5 smaller than one given by (34). Comparing the "triple" self-energy with the Brueckner one (20) we find that the "triple" self-energy is by a factor 7 smaller. This is already enough to neglect the "triple" contribution. However we would like to demonstrate that suppression of the "triple" contribution is even stronger: its influence on the point of phase transition is exact(!) zero in linear in x approximation. This interesting fact is related to anomalous "triple" self energy shown in Fig. 6b. Simple consideration based on the structure of the vertex (32) shows that following exact relation takes place

$$\Sigma_{3a}(\mathbf{q}_0, 0) = -\Sigma_{3n}(\mathbf{q}_0, 0). \tag{35}$$

According to (8) the magnon spectrum found without "triple" diagram is of the form

$$\omega_{\mathbf{q}} \propto \sqrt{\tilde{A}^2 - \tilde{B}^2}, \tag{36}$$

where $\tilde{A}$ arises from the normal terms in the effective Hamiltonian and $\tilde{B}$ arises from the anomalous terms. At the critical point $\tilde{A} = -\tilde{B}$ and hence the excitation energy vanishes. With account of "triple" diagrams the relation (36) should be rewritten as

$$\omega_{\mathbf{q}} \propto \sqrt{\left(\tilde{A} + \Sigma_{3n}\right)^2 - \left(\tilde{B} + \Sigma_{3a}\right)^2}. \tag{37}$$

It is clear that because of (35) the dispersion (37) vanishes exactly at the same point as (36). This proves our statement that the "triple" self energy does not influence position of the transition point. However away from the transition point when the spin-wave gap is increasing the "triple" self energy is getting more important. Note that similar situation takes place with "triple" diagrams considered in Ref.[9] for $J_1 - J_2$ model.